Imaging and Analysis of Nanowires

DAVID C. BELL,[1,2]* YUE WU,[3] CARL J. BARRELET,[3] SILVIJA GRADEČAK,[3] JIE XIANG,[3] BRIAN P. TIMKO,[3] AND CHARLES M. LIEBER[2,3]

[1]*Center for Imaging and Mesoscale Structures, Harvard University, Cambridge, Massachusetts 02138*
[2]*Division of Engineering and Applied Sciences, Harvard University, Cambridge, Massachusetts 02138*
[3]*Department of Chemistry and Chemical Biology, Harvard University, Cambridge, Massachusetts 02138*

KEY WORDS HRTEM; STEM; microanalysis; nanotechnology

ABSTRACT We used vapor-liquid-solid (VLS) methods to synthesize discrete single-element semiconductor nanowires and multicomposition nanowire heterostructures, and then characterized their structure and composition using high-resolution electron microscopy (HRTEM) and analytical electron microscopy techniques. Imaging nanowires requires the modification of the established HRTEM imaging procedures for bulk material to take into consideration the effects of finite nanowire width and thickness. We show that high-resolution atomic structure images of nanowires less than 6 nm in thickness have lattice "streaking" due to the finite crystal lattice in two dimensions of the nanowire structure. Diffraction pattern analysis of nanowires must also consider the effects of a finite structure producing a large reciprocal space function, and we demonstrate that the classically forbidden 1/3 {422} reflections are present in the [111] zone axis orientation of silicon nanowires due to the finite thickness and lattice plane edge effects that allow incomplete diffracted beam cancellation. If the operating conditions are not carefully considered, we found that HRTEM image delocalization becomes apparent when employing a field emission transmission electron microscope (TEM) to image nanowires and such effects have been shown to produce images of the silicon lattice structure outside of the nanowire itself. We show that pseudo low-dose imaging methods are effective in reducing nanowire structure degradation caused by electron beam irradiation. We also show that scanning TEM (STEM) with energy dispersive X-ray microanalysis (EDS) is critical in the examination of multicomponent nanowire heterostructures. *Microsc. Res. Tech. 64: 373–389, 2004.*

INTRODUCTION

Richard Feynman's 1959 lecture entitled "There's Plenty of Room at the Bottom" is a source of inspiration for nanotechnology. During this lecture, Feynman foresaw the importance and application of electron microscopy. Looking back at this lecture, the prediction was uncanny, given that the imaging of nanostructures using electron microscopy has played a critical role in the development of nanoscience, not to mention acting as a catalyst for further developments in electron microscope instrumentation. A beautiful example of nanoscale imaging was the discovery of the carbon nanotube using HRTEM by Sumio Iijima (1991). Nanoscale objects are by definition small (having dimensions in the nanometer scale), their physical properties being different from the corresponding bulk material; similarly, the imaging of these objects presents the need for new microscopy techniques. One-dimensional nanostructures such as nanowires have stimulated great interest due to their importance in fundamental scientific research and their potential new technology applications (Lieber, 2003). Studies to date have shown that these attractive nanowire building blocks can be assembled into nano-electronic and photonic devices including field-effect transistors (Cui and Lieber, 2001), logic gates (Huang et al., 2001b), decoders (Zhong et al., 2003), sensors (Cui and Lieber, 2001), light-emitting diodes (Duan et al., 2001), photodiodes (Wang et al., 2001), and laser diodes (Duan et al., 2001). The emergence of nanotechnology and the development of these fascinating applications rely on the rational control over the electronic and optical properties of nanowires and the chemical synthesis (including the adjustment of the morphology, size, and material composition in various nanowire structures), all of which can only be observed by electron microscopy due to the finite size of nanowires. TEM and STEM imaging and analysis are critical for the future developments of nanowire-related structures and devices. This article describes the electron microscope techniques that we have developed to enable the characterization of nanowires both structurally and compositionally and to discuss the challenges and difficulties involved.

From our experience, the characterization of nanowires takes place in two stages. The first stage focuses on the synthesis and development of the desired nanowire building block, with electron microscopy providing a feedback to rationally grow the desired nanowire. Compositional information of the nanowires can be obtained using energy dispersive X-ray analysis (EDS). General nanowire structural information, such as how

*Correspondence to: David C. Bell, Center for Imaging and Mesoscale Structures, Harvard University, 7 Divinity Ave., Cambridge MA 02138.
E-mail: dcb@deas.harvard.edu

Received 2 July 2004; accepted in revised form 27 August 2004
DOI 10.1002/jemt.20093
Published online in Wiley InterScience (www.interscience.wiley.com).

thick the nanowires are and if the nanowires are single crystal or amorphous, can readily be determined using TEM. Both TEM and EDS characterization provide the necessary inputs to tune the synthesis parameters to produce the desired building block. The second stage starts once the synthesis of the desired building block has been achieved. At this point, more advanced techniques are used to investigate the structure and properties of the nanowire. A thorough characterization includes the determination of the growth direction, cross-section, surface morphology, dislocations, and stacking faults. Determination of the nanowire growth direction and cross-section are important to further our understanding of the surface energetics and the mechanisms of the crystal formation using a catalyst-based synthesis process. Moreover, they provide an understanding of the material properties that affect the electronic or optical response of a nanowire fabricated device.

The imaging and analysis of nanowires with electron microscopy also involves an understanding of the limitations of standard imaging and analysis techniques and how they can be applied to nanoscale objects. The techniques that we describe herein differ from the standard imaging and analysis techniques involved when characterizing bulk materials. It is possible to form incorrect structure determinations if the presence of forbidden reflections in the diffraction patterns of silicon nanowires are not correctly taken into account, and the description of these reflections are detailed in this article. Other considerations, such as beam damage, can affect the HRTEM images, and also change the compositional information obtained using EDS. Nanowires are finite objects and their imaging and analysis requires a new approach to the methodology of diffraction studies, HRTEM, and analytical microanalysis.

We organized the article into four broad topics: Nanowire Synthesis; Experimental Techniques; Discussion; and Conclusion. In the section entitled Nanowire Synthesis, we discuss the principles of synthesis of single composition nanowires, axial heterostructures, and core-shell nanowires. We then move through a discussion of our experimental techniques, detailing nanowire sample preparation; HRTEM imaging of nanowires; image artifacts such as image delocalization and incorrect lattice spacings; nanowire HRTEM image simulations; diffraction studies, demonstrating the large reciprocal space function of the nanowire; and microanalysis of nanowires. This is followed by a discussion of HRTEM imaging and the possible effect of crystal faceting, anomalous diffraction from nanowires, and microanalysis, and finally we present a summary of our conclusions.

NANOWIRE SYNTHESIS: THE MAIN CONCEPTS

Most nanowire syntheses we have undertaken are based on the VLS growth mechanism as summarized by Lieber (2003). In this mechanism, a nanocluster is used as a catalyst and exposed to carefully designed precursor vapor (V). The phase diagram of the catalyst (S) and the decomposed precursor determines the temperature and pressure required to form a liquid alloy droplet (L) from the nanocluster. As more of the precursor incorporates, the nanocluster supersaturates and initiates a crystal nucleation process, which results in an axial growth of the solid nanowire (S). A direct observation of VLS nanowire growth has been reported using TEM by Wu et al. (2001). By choosing monodisperse nanoclusters as catalysts, the size of the liquid alloy droplets can be confined and yield nanowires with narrow diameter distribution and a close correlation between the nanowire diameter and initial nanocluster size as reported previously (Gudiksen, 2000; Cui et al., 2001; Wu et al., 2004b). One of the main examples is the synthesis of silicon nanowires using differing sizes of monodisperse gold (Au) nanoparticles as catalysts and silane (SiH_4) as the vapor-phase precursor as shown in Figure 1a. A eutectic droplet of Au and Si stays at one end and serves as a catalyst particle (Fig. 2a), setting a size limit for nanowire diameter. TEM studies (Gudiksen and Lieber, 2000) have shown that by this means silicon nanowires with a narrow diameter distribution can be synthesized ranging from several nanometers to tens of nanometers (Fig. 2b,c). Using similar synthesis techniques, nanowires of differing elemental composition can be obtained, such as silicon, germanium, gallium nitride, or cadmium sulfide, although depending on the required end product the synthesis method can vary from chemical vapor deposition (CVD) to a laser ablation technique. Nanowire axial heterostructures are nanowires that have a modulation in composition along their lengths, as shown in Figure 1b. In the planar

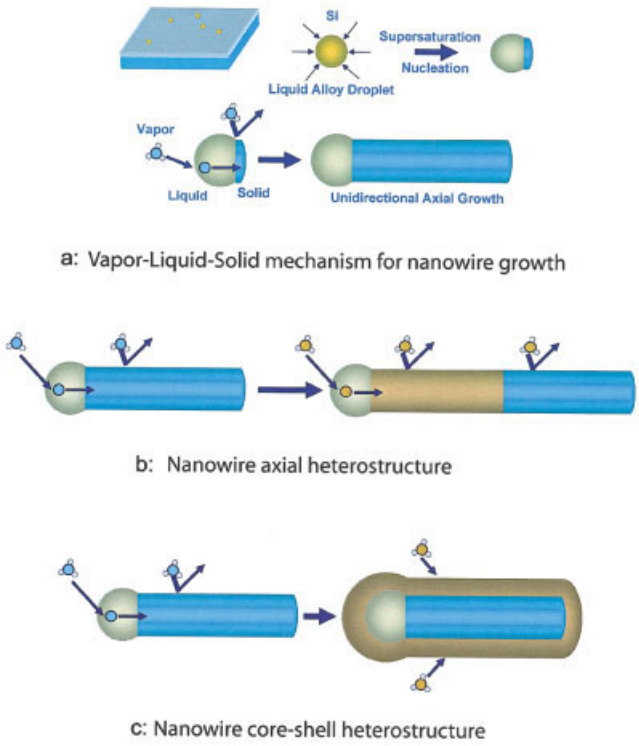

Fig. 1. Illustrations of nanowire synthesis process. **a:** Vapor-liquid-solid (VLS) mechanism for nanowire growth. **b:** Synthesis method to form nanowire axial heterostructure. **c:** Synthesis method for nanowire core-shell heterostructure formation.

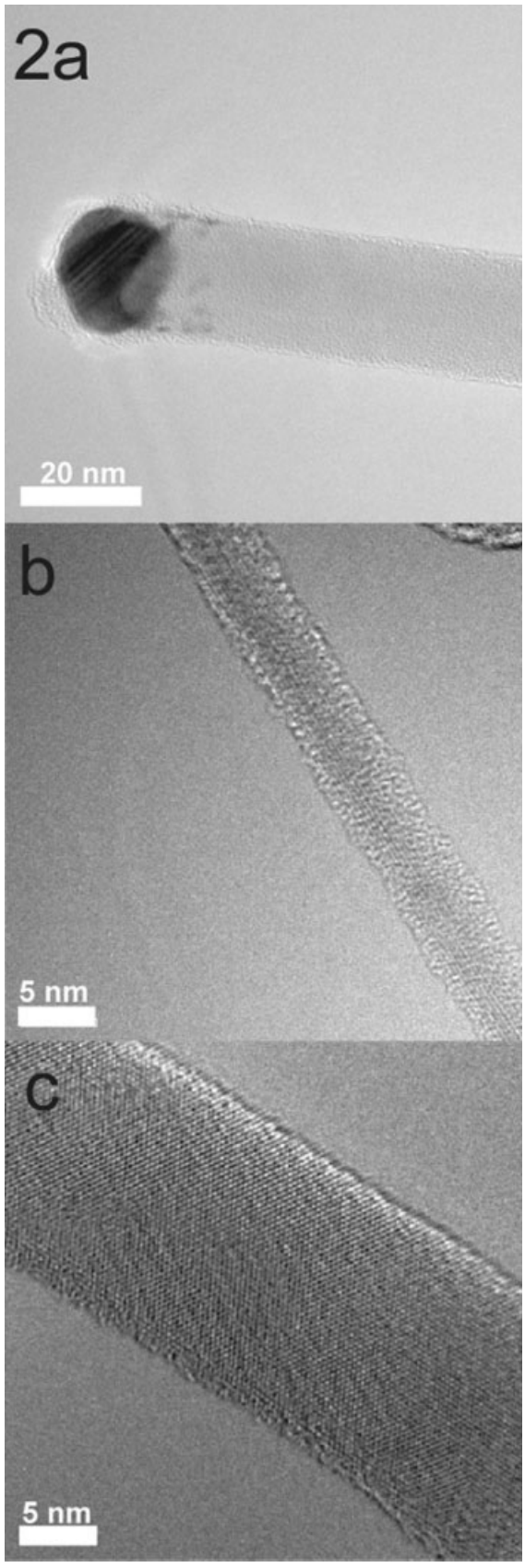

semiconductor industry, compositionally modulated thin film structures have been developed for electronics and photonics applications. By changing the composition along the nanowire, new opportunities for band-gap engineering and dopant modulation are possible at the nanoscale. The synthesis of nanowire axial heterostructure involves changing the types of precursors during the nanowire growth. For example, during silicon nanowire CVD growth, by switching the dopant precursor from diborane (B_2H_6) to phosphine (PH_3) while keeping the silane (SiH_4) precursor flowing, a complementary doping along a single silicon nanowire can be made with a p-n junction in a single nanowire. By similar approaches, GaAs/GaP, InAs/InP, and Si/SiGe nanowire axial heterostructures can also be prepared for photonic and electronic applications.

A third type of complex nanowire structure is called a core-shell nanowire heterostructure, which has a modulation in elemental composition along the nanowire radius. The changing of the precursors during the nanowire growth is similar to the axial heterostructures synthesis; however, the preference of synthesizing a core-shell structure over an axial heterostructure can be achieved by shifting the growth temperature and pressure. This relates to employing a much higher homogeneous precursor decomposition rate on the nanowire surface than the axial growth rate as shown in Figure 1c. By changing the different reactants and dopants, it is possible to produce multiple shell structures of differing compositions. Many examples with core-shell compositions such as Ge/Si, Si/Ge, and p-Si/SiO_2 core-shell structures have been demonstrated.

One of the purposes of these synthesis techniques is to produce nanowire-based functional devices. The scope of such devices ranges from basic electronic devices like field-effect transistors (FETs) (Cui et al., 2001), logic gates (Huang et al., 2001a,b), decoders (Zhong et al., 2003), and sensors (Cui et al., 2001) to optoelectronic devices like light-emission diodes (Duan et al., 2001), photodiodes (Wang et al., 2001), and laser diodes (Duan et al., 2001). In these devices, either a single nanowire with a source-drain contact or crossed nanowires with a source-drain contact on each of the wires is used. For example, in the case of nanowire FETs, a single silicon nanowire can be used as a building block, the nanowire FET can be switched on and off by either the back gate of a heavily doped silicon wafer or a top gate of lithographically defined metal line crossing the nanowire. This kind of nanowire FET has become the basis of other nanoelectronic devices including logic gates, decoders, sensors, and memories. More complex devices, such as nanoscale optoelectronic devices, employ two crossed nanowires with one the p-type silicon nanowire and the other a direct band-gap compound semiconductor nanowire, such as a CdS or GaN nanowire. In this way, taking advantage of a bottom-up approach of using building blocks to assem-

Fig. 2. HRTEM images of silicon nanowires. **a:** Silicon nanowire showing attachment of gold catalyst particle on the end. **b:** Thin ~5 nm silicon nanowire showing lack of contrast along edges, but atomic structure information indicated along the length of the wire. **c:** Silicon nanowire ~17 nm wide; micrograph shows clear atomic structure detail.

ble functional nanoscale devices, the desire is to integrate as many functions as possible into the fundamental building block components.

EXPERIMENTAL TECHNIQUES
HRTEM Imaging of Nanowires

HRTEM of nanowires and nanowire devices follows from high-resolution imaging methods such as those described by Williams and Carter (1996) and Spence (1981), with adaptations of imaging methods required due to the finite nature of the samples. Since some of our nanowires can be thinner than 6 nm, imaging becomes problematic due to the lack of total atom density (dependent, of course, on the atomic number of the material involved), and hence lack of scattering elements to produce a suitable phase contrast image. Adjustment of the objective lens defocus to obtain optimum imaging conditions and hence sufficient contrast to record the micrograph is problematic, and objective lens defocus values which deviate from an instrumental optimum can lead to other imaging issues that we detail below. Tilting nanowires to a required zone-axis needed for HRTEM imaging is also difficult due to the large reciprocal space function from the thin diameter of the wire. Apart from imaging nanowires dispersed on a TEM grid, we have previously demonstrated that HRTEM imaging of a nanowire cross section can be achieved by embedding nanowires into epoxy and microtoming the nanowire/epoxy solid mixture as described in Wu et al. (2004b).

Experimentally, the nanowires that have been synthesized as previously described are mechanically removed from the growth substrate and dispersed into 2-propanol, which is then droppered onto a TEM grid with lacey or holey carbon support film. Lacey carbon is suitable when the nanowires are longer than 10 microns. For shorter nanowires, holey carbon or a plain support film is often preferred to increase surface area for securing nanowires for observation. Another method for removal of the nanowires from the substrates involves sonication of the substrate in ethanol and then dispersion onto the lacey carbon TEM grids. HRTEM imaging of our synthesized nanowires was made using a JEOL 2010F TEM operating at 200 kV. Prior to insertion, the TEM sample and holder rod were prepumped with a Fischione 1020 pumping station for 20 minutes to ensure complete removal of remaining solvents or water contamination. A thin silicon nanowire of order 5 nm in diameter can amorphize in less than a minute under a 200 kV electron beam; thus, the thinner the wire the faster the damage, as Figure 5a,b indicates for a ZnS nanowire. We therefore developed an imaging protocol based on low-dose microscopy techniques in order to minimize the effects of beam damage on the crystalline structure of the sample. In our method, the focusing and crystal zone-axis orientation are performed on an adjacent region of the sample. In the case of a nanowire, the most logical position for these alignments are further along the wire length from the area of interest; the sample is then moved to the area of interest and the HRTEM micrographs quickly recorded.

Figure 2a shows a single silicon nanowire with a gold catalyst particle still attached to one end, the other end of the wire that is not shown is anchored to a holey carbon support film. Figure 2b presents an HRTEM image of a thin ~5 nm silicon nanowire indicating some of the problems of nanowire image interpretation. In this image the core region of the wire appears crystalline, while the edges appear amorphous; it is unclear from this image if the wire edges are actually amorphous or if the structure of the edges only appears amorphous due to the lack of atomic scattering needed to produce a phase contrast image. Figure 2c shows a silicon nanowire; this wire is 17 nm wide and the image shows clear atomic structure detail, similar to what would be observed from a bulk single crystal silicon sample.

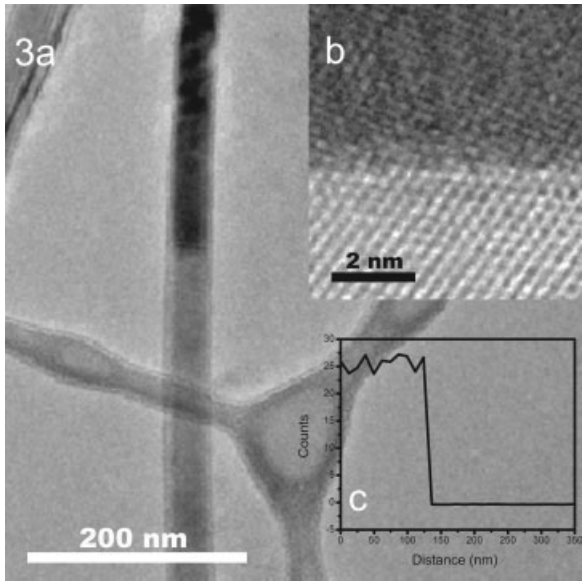

Fig. 3. NiSi/Si nanowire axial heterostructure. **a:** TEM image of the nanowire device clearly showing the junction between NiSi and Ni. **b:** HTREM image of the atomically sharp metal-semiconductor junction of NiSi/Si. **c:** EDS linescan taken along the length of the nanowire showing the junction as a function of characteristic Ni-K X-ray line.

Other nanowire systems have been examined with HRTEM. Figure 3a shows a TEM image of an NiSi/Si nanowire axial heterostructure; in this image the metallic nickel silicide section of the nanowire appears clearly dark with a well-defined junction to the silicon section. Figure 3b shows the corresponding HRTEM image of the NiSi/Si interface; from such an image the degree of lattice misfit can be calculated following conventional TEM methods as applied to semiconductor materials. This method of image analysis has been previously shown to be possible for the case of nanowires by Lauhon et al. (2002) and Gudiksen (2002). We also imaged core-shell nanowire structures with HRTEM. Figure 4a,b shows a core-shell heterostructure; the core is a 20-nm n-doped silicon nanowire grown from a gold catalyst via the VLS mechanism as described previously. The shell is intrinsic Ge that was deposited by CVD. HRTEM allows for a detailed examination of the interface between the Si and Ge (Fig. 4c) and, combined with selected area diffraction patterns, these images allow the degree of lattice misfit along the boundary to be determined, an important factor for

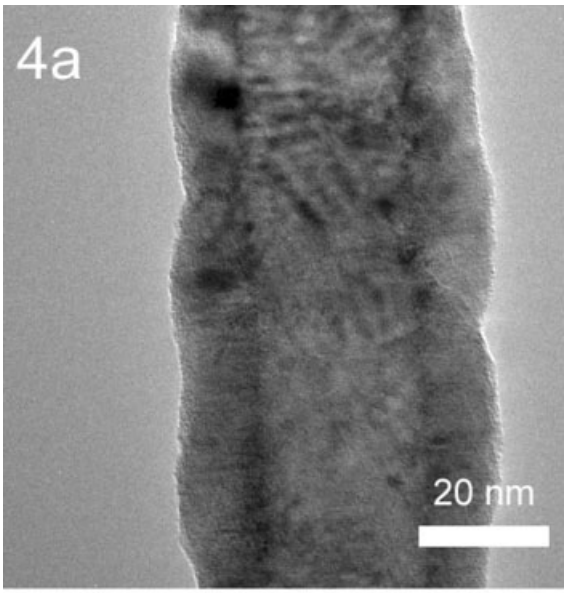

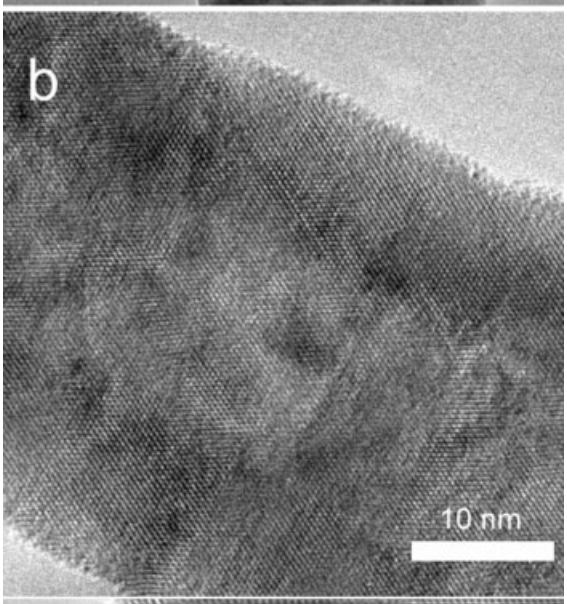

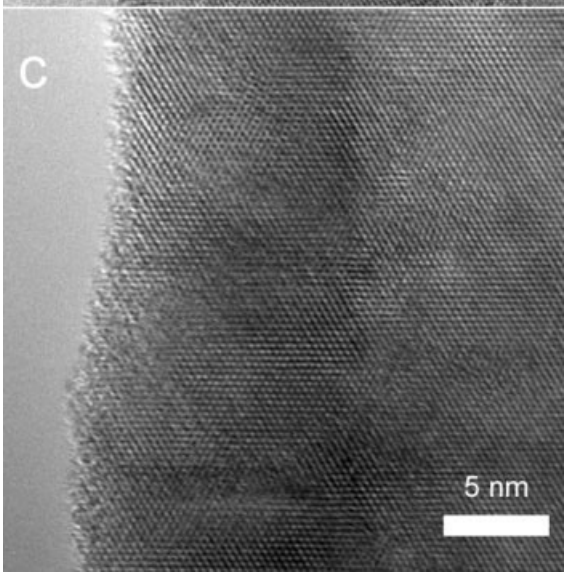

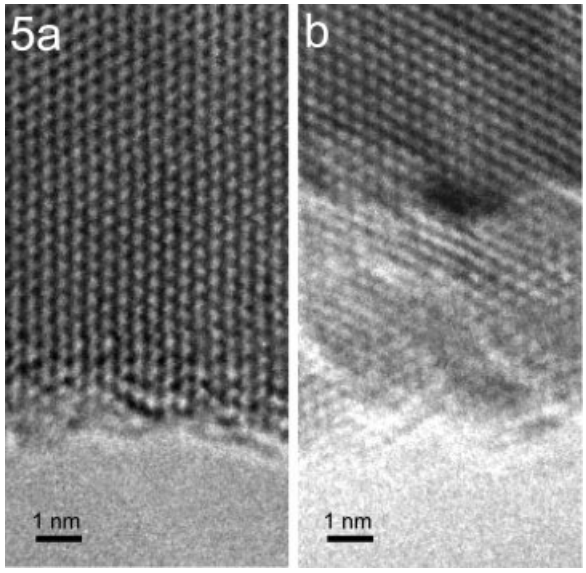

Fig. 5. HRTEM images of ZnS nanowire. **a:** HRTEM image of nanowire edge showing atomic structure information. **b:** HRTEM image of nanowire edge after several minutes of 200 kV electron beam irradiation.

relating nanoscale structure to electronic device function.

Imaging nanowires using a thermal field emission microscope, such as the JEOL 2010F used in this study, can also lead directly to "artifacts" in the HRTEM nanowire images. Should the microscope operating conditions not be properly considered, for instance, if the chosen objective lens underfocus value is significantly away from an optimum "close to" Scherzer defocus value, the micrograph can show image delocalization, where the lattice image is displaced from the apparent sample (Otten and Coene, 1993). Although this effect is not limited to the examination of nanowires, it becomes readily apparent that even small amounts of delocalization will be easily noticeable in the recorded micrograph due to the finite width of the wire. Without correctly considering the setting of the objective lens underfocus value, lattice fringes are noticeably formed outside the borders of the nanowire itself and usable phase contrast is lost from the image of the wire. We have demonstrated this effect as shown in Figure 6, when imaging a silicon nanowire and adjusting the objective lens defocus to 200 nm below the microscopes Scherzer value. Since for imaging nanoscale objects, phase contrast is small initially, this effect needs to be aggressively minimized. From Lichte (1991) the optimum value of underfocus to minimize image delocalization should be:

$$\Delta f_{\text{opt}} = -MC_S\lambda^2 u_{\max}^2$$

Fig. 4. TEM images of Ge/Si core-shell nanowire. **a:** The Si core which is a 20 nm n-doped nanowire grown from a gold catalyst via the VLS mechanism. **b:** TEM image of the nanowire with clearly defined shell structure. **c:** HRTEM image of the shell which is intrinsic Ge that was deposited by CVD.

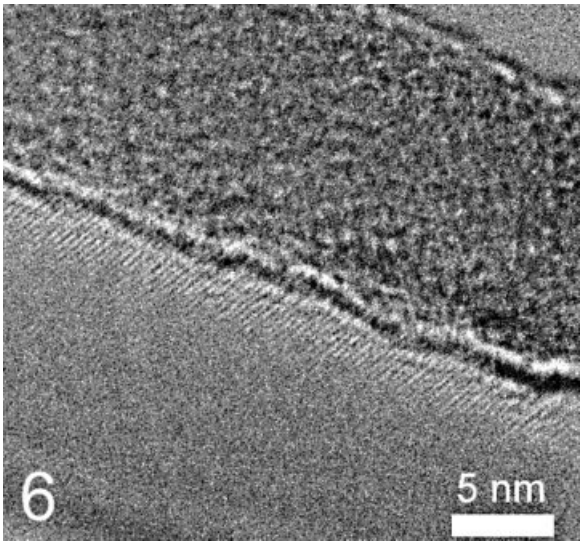

Fig. 6. HRTEM image of a 10 nm silicon nanowire showing image delocalization.

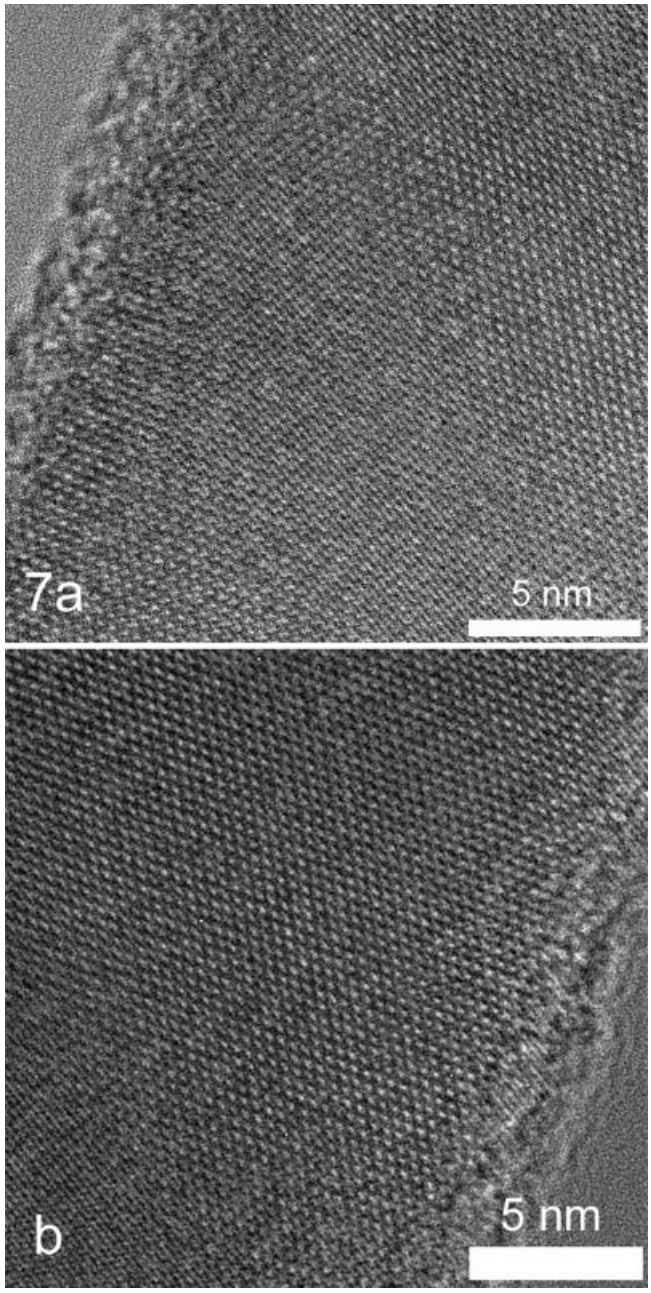

Fig. 7. HRTEM images of a silicon nanowire. **a:** Aligned along the [111] zone axis. **b:** Tilted slightly <1° away form the [111] zone axis and having "deceptive lattice spacings."

where M is an operational value actually determined by the cut-off value chosen for u (spatial frequency) and has a value between 0.75 and 1. For our JEOL 2010F, which has a spherical aberration value (C_s) of 1.0 mm, and operating at 200 kV, a typical range of underfocus values for the objective lens should be between –70 nm to –50 nm, to minimize the effects of delocalization (at suitable spatial frequencies corresponding to d_{110} of Si of 0.34 nm), which fortunately encompasses the extended Scherzer defocus value (for our microscope it is –61 nm). As stressed by Williams and Carter (1996), image delocalization can only be minimized in a field emission TEM, but not eliminated.

Other HRTEM nanowire imaging "artifacts," such as incorrect "lattice spacings" caused by the large reciprocal space function, can be avoided. Using the breakdown of the weak phase object (WPO) approximation to indicate correct alignment of the zone-axis, it is possible to know when the spacings in the HRTEM image can be reasonably trusted. Malm and O'Keefe (1997) described this effect when imaging nanocrystalline palladium particles by conducting image simulations at various tilts and defocus values. In this article, the authors argue that a nanoscale crystal oriented within a few milliradians of the zone-axis will show white dots centered on black dots, indicating that the WPO has broken down and that the image is close to the zone-axis, and hence the measured lattice spacings of the HRTEM or "structure image" will be near the correct values. Tilting away from the zone-axis can produce what appears to be an atomic structure image far away from the zone-axis that has apparent spacings that can deviate by up to 10%. We have experimentally observed these effects when imaging silicon nanowires that are tilted away from a defined zone-axis. With the microscope magnification previously being calibrated with a bulk crystal sample, Figure 7a shows a silicon nanowire tilted $\cong 1°$ away from the [111] zone-axis orientation and shows fine lattice spacings that when measured from the micrograph indicate a distance in the 0.21–0.24 nm range (interestingly dependent on fringe orientation), the corresponding value for d_{220} = 0.19 nm. Figure 7b shows the same wire tilted to zone-axis orientation with the lattice spacing measured as 0.19 ± 0.01 nm, as expected. It should be noted that it is possible to measure lattice spacings differing from published values due to chemical or structural changes (perhaps due to beam irradiation) or strains present in the material, so the experimental procedure should be

repeated several times to confirm the reproducibility of the results.

Nanowire HRTEM Image Simulation

The finite diameter of the wires, especially wires which are <6 nm, produce "nanoscale imaging" effects that need to be considered when recording HRTEM micrographs and either confirmed and understood or dismissed when interpreting the HRTEM structure images. Complete HRTEM "structure image" understanding must include the corresponding multislice image simulations for the particular thickness and defocus values employed. We have found that the HRTEM image simulations of very thin nanowires must be based on a modified multislice approach, which needs to include the effects of the reducing number of atoms towards the edge of the wire, such as previously discussed above and outlined for nanomaterials by Nihoul et al. (1998), and perhaps more importantly, must include consideration for the large reciprocal space function which corresponds to the wire's thin diameter. The symmetry of the wire allows the calculation to employ a modified two-dimensional shape function; our periodic object being modeled is now finite in two dimensions. The Fourier transform for a nanowire oriented along the x direction becomes:

$$\mathrm{V}(x, y, z) = \mathrm{V}(\mathbf{y}) = \boldsymbol{FT}\,[\mathrm{V}(\mathrm{u})]$$

where we have assumed that z is the direction of the incident electrons, and u is the associated vector in Fourier space corresponding to the real space vector y. Modifying the multislice algorithm directly is possible, but a more useful approach to the finite size problem is defining a modified crystal unit cell that produces the same effect and can be achieved easily. In this approach, the unit cell is a modified crystal unit cell that encompasses the width of the wire and slightly beyond it into "free space" (Fig. 8) and then propagating that cell along the required wire length before inputting into the multislice algorithm of choice. In our case, we created a small algorithm that required defining the wire width and desired length, elemental components, and base unit cell structure; the output from this is a data file that can be read into the multislice algorithm, in our case the Electron Microscopy Image Simulation (EMS) for which a Java-based version is available online (Stadelmann, 1995) or the original EMS program (Stadelmann, 1987).

HRTEM image simulations of nanowires are shown in Figures 9 and 10; the numbers on the image simulation inset reflect defocus/thickness values for the simulation. The thickness values were chosen to correspond closely to the wire diameter. Unlike bulk or infinite crystal image simulation, where the crystal thickness is estimated from the simulation, nanowire simulation is actually more defined, since the thickness of the wire is within several nm of the diameter. The possible thickness range is reduced and the objective lens defocus value is obtained from the microscope; hence, image simulation parameters are well defined. Simulation of the CdS nanowire (Fig. 9) was performed by assuming an infinite crystal; this nanowire is relatively thick and the atomic structure image indicated

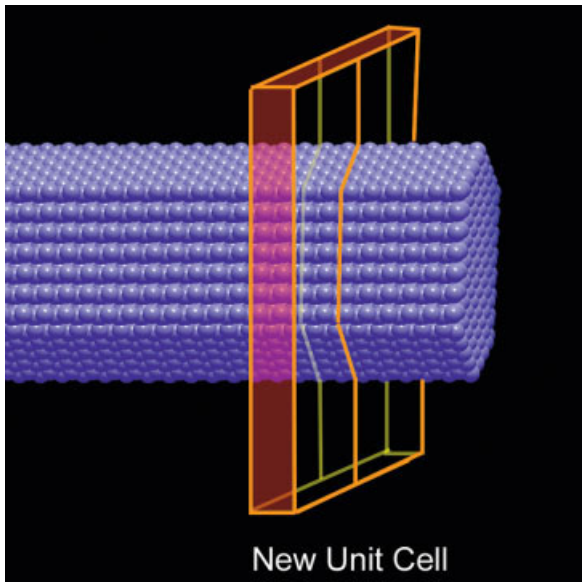

Fig. 8. Illustration of the new unit-cell definition for input into an electron multislice simulation program.

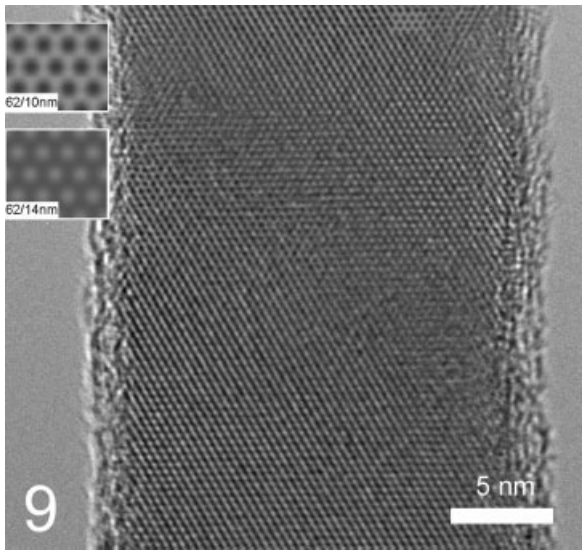

Fig. 9. HRTEM image of CdS nanowire; the inserts are multislice simulations with the indicated values of objective lens defocus/crystal thickness in nanometers.

well-defined 2D fringes. Correspondingly, we discovered that image simulation of silicon nanowires that are thicker than 6 nm can be performed under the assumption of an infinite crystal (Fig. 10a,b). If, however, the silicon nanowire is 6 nm or less, then the structure image recorded shows a pseudo 1D lattice fringe effect or "streaking" as a result of the large reciprocal space function (Fig. 10c,d). In this case the modified multislice unit cell algorithm (Fig. 8) was used to produce the matching simulations as indicated. It is of course possible to have 1D lattice fringes in any HRTEM image; however, a corresponding image sim-

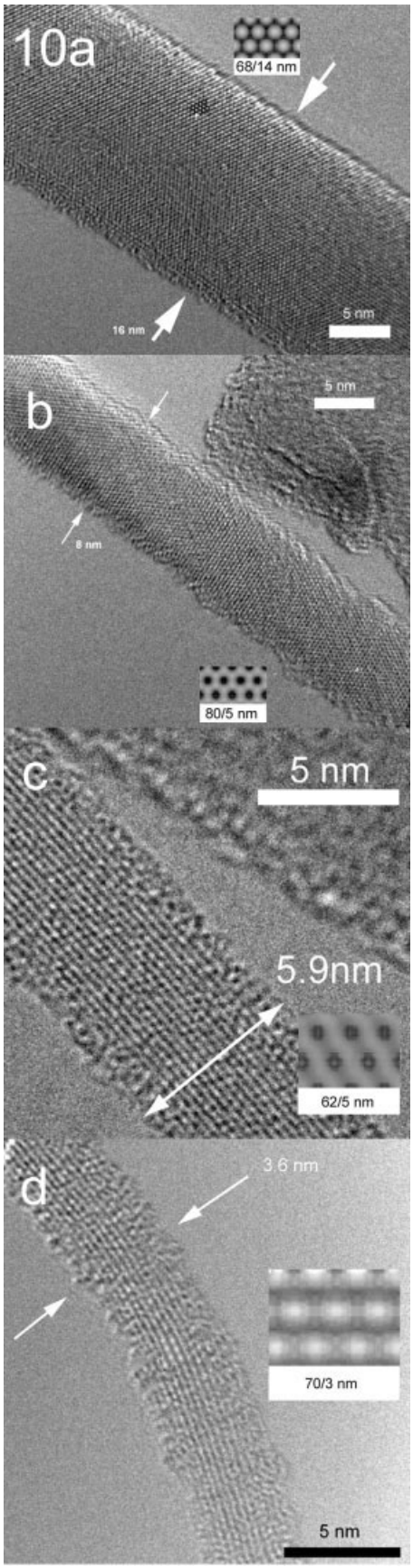

ulation at the same defocus and thickness values of a thin film sample shows only a well-defined 2D atomic structure image.

Diffraction Studies of Silicon Nanowires

Because the reciprocal space function of the nanowire is large corresponding to the "thinness" of the nanowires, the interception of the diffracted beams with the Ewald sphere can occur at angles significantly away from a zone axis, and still produce a diffraction pattern that at first appears to be zone axis-oriented. A slightly converged incident electron beam will produce in diffraction space rods rather than the typical convergent beam disks, as shown in Figure 11, which is a silicon nanowire that has been initially tilted to a [111] zone-axis orientation. Indexing of this zone-axis orientation is presented in Figure 15b; note that this pattern shows reflections present at the $\frac{1}{3}\{\bar{4}22\}$ positions that should be classically forbidden. A possible explanation for the presence of these reflections is presented in the Discussion section.

The large reciprocal space function of the silicon nanowire has been experimentally demonstrated by performing a sequence of tilting experiments along the nanowire's radial and longitudinal axis. For this tilt series we used a Fischione Instruments advanced tomography holder that has a tilt limit of $\pm 75°$ on our microscope.

In the initial sequence of experiments we found that tilting longitudinally (along the length of the wire) produces changes in the diffraction pattern that match the equivalent tilting of a bulk or equivalently infinite sample and the diffraction pattern changes rapidly as the Ewald sphere rotates, indicating well-defined changes of the reflections at all orders of Bragg diffraction, as illustrated by the series of images in Figure 11.

By performing the second tilting experiment orthogonally to the longitudinal axis, i.e., tilting radially around the wire axis, the nanowire diffraction pattern indicates a slowly changing pattern when compared to the above for the equivalent tilt angle, as indicated in Figure 12. This is due to the large reciprocal space function—in this direction the diffracted beams intersect the Ewald sphere and produce significant intensity at larger angles than the corresponding bulk sample diffraction pattern. Figure 12 indicates that it is not until the tilt is greater than 20° away from the initial [111] zone-axis orientation that the {220} reflections become noticeably absent, further tilting to 50° completes the change of all orders of diffracted beams. This also demonstrates that the orientation of the nanowire to a precise zone-axis in reciprocal space becomes problematic: higher-order reflections must necessarily be used to correctly ascertain zone-axis alignment. Figure 12 shows the higher-order reflection effects; at 20° tilt

Fig. 10. HRTEM images of silicon nanowires of varying thicknesses and inserts are the corresponding multislice simulations. **a,b:** Simulations of thick nanowires can be modeled as for the bulk materials. **c,d:** Simulations of thin wires less than 6 nm are modeled using the modified unit cell approach and show "streaking" that matches the HRTEM image. The indicated values of objective lens defocus/crystal thickness are in nanometers.

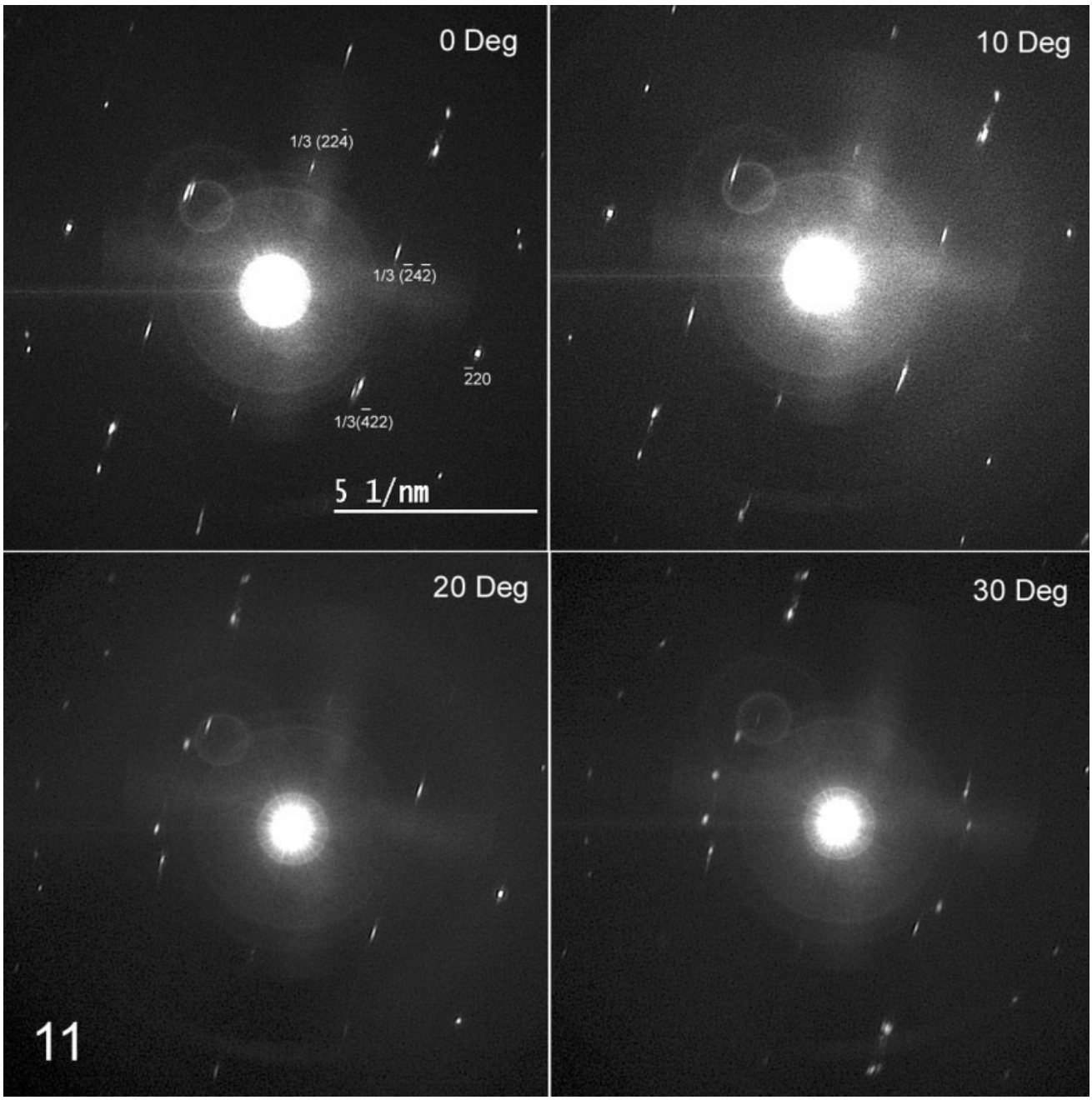

Fig. 11. Diffraction patterns at indicated sample tilt angle, taken from a silicon nanowire (starting at [111] zone-axis orientation) tilted along the nanowire longitudinal axis.

and greater from the initial zone axis the (220) reflections do not appear to be symmetrical. If we were to show a wider field of view we would still observe this effect at low tilt angles, but notably only with very high order Bragg reflections. Note that tilting 30° degrees off zone-axis still shows the presence of the forbidden $\frac{1}{3}\{\bar{4}22\}$ reflections, which could contribute to an incorrect zone-axis alignment needed for HRTEM studies in silicon nanomaterials along the [111].

The above experiments indicate that the higher-order reflections being produced from the larger Bragg scattering angles are correspondingly more sensitive to changes in sample tilt, and should be considered to ascertain a correct zone-axis alignment.

Microanalysis of Nanowires

Complex nanowire systems require characterization by microanalysis techniques so as to provide a feedback

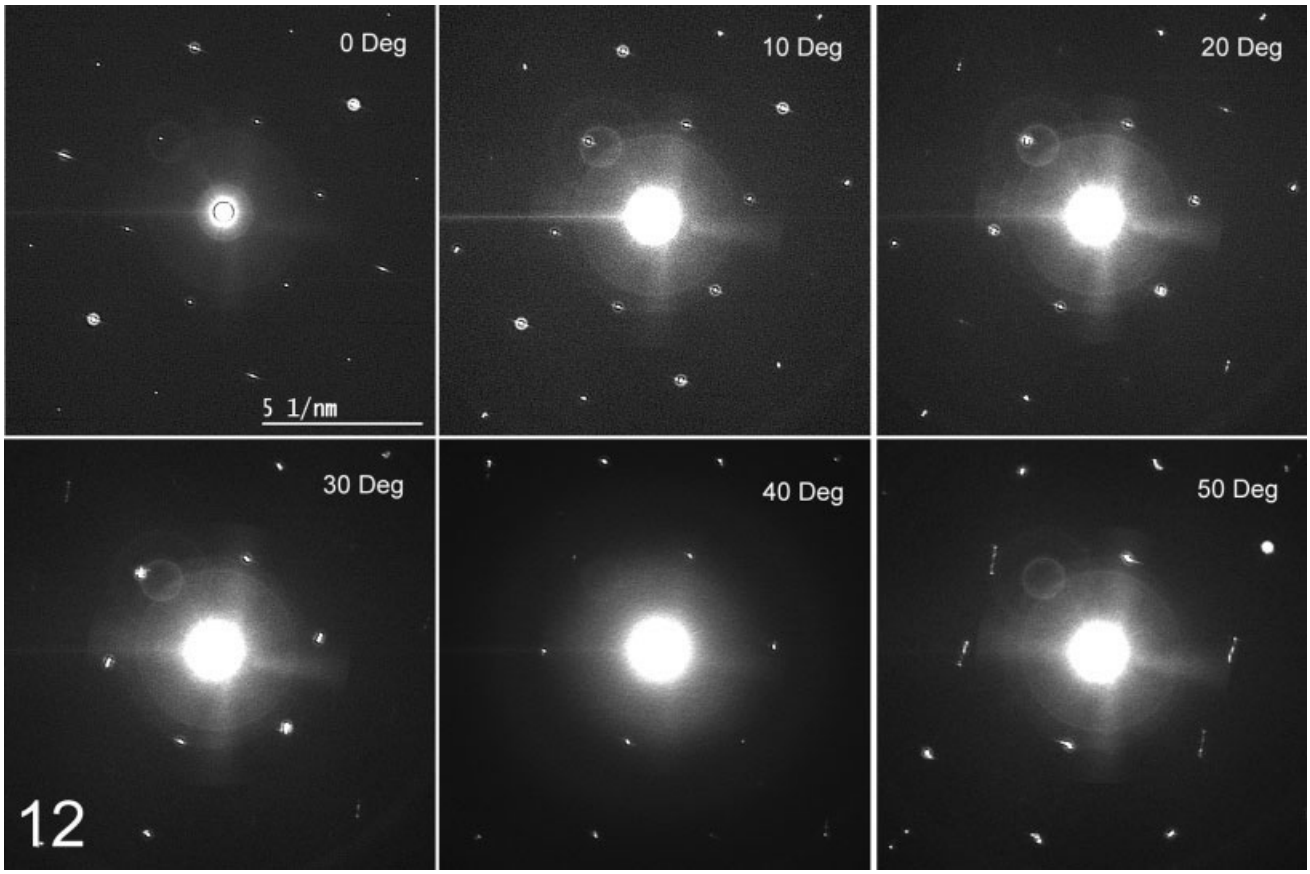

Fig. 12. Diffraction patterns at indicated sample tilt angle, taken from a silicon nanowire (starting at [111] zone-axis orientation) tilted along the nanowire radial axis, indicating lack of significant low-order beam change until the sample has been tilted 20° from zone-axis.

on the synthesis process and to gain insight into the chemical composition of the resultant nanowire structures. Typically, microanalysis is performed using a TEM or STEM fitted with a EDS system; with such a system, characteristic EDS spectra, EDS linescans, and elemental or spectral maps can be obtained. Complex nanowire devices such as core-shell structures are best examined using STEM and EDS with elemental line profiles acquired along or across the nanowire and spectrum images or maps of the overall structure. EDS spectrum imaging in particular is a valuable technique to provide understanding of the resultant synthesis processes and nanowire structures, which is further detailed in this article.

For our experiments we employed a Vacuum Generators HB-603 dedicated STEM or a JEOL 2010F operating in STEM mode. Spectrum imaging obtained of an axial nanowire heterostructure consisting of zinc sulfide (ZnS) and zinc selenide (ZnSe) shows a uniform distribution of zinc along the whole wire (Fig. 13b), while the elements selenium (Fig. 13c) and sulfur (Fig. 13d) are concentrated at the opposite side of the junction. Figure 13a shows the corresponding brightfield image of the nanowire. In this particular wire we show that the sulfur and selenium diffused towards each other in the heterostructure and made a moderated structural transition, rather than similar abrupt transitions, as in the case of an Ni/NiSi nanowire. We have also found that STEM can be used to analyze the chemical composition distribution in a core-shell nanowire structure such as the type shown by the brightfield image of an Si/CdS core-shell nanowire (Fig. 14a). For the Si/CdS core-shell nanowire structure, the EDS spectrum (Fig. 14g) and spectrum images were obtained using a JEOL 2010F operating in STEM mode. These images clearly show that sulfur (Fig. 14c) and cadmium (Fig. 14d) concentrated in the shell region, while silicon (Fig. 14b) was concentrated only in the core region.

Compared with the case of axial heterostructures, it is more complicated to determine the interface between different compositions due to the overcoating of shell. To extract this type of information, we employed EDS line profiles across the wire diameter and the line profiles were then modeled by assuming a Gaussian electron probe profile. In Figure 14e,f, the Cd-L (red) and Si-K (blue) line profiles, markers were the measured values and solid lines were calculated profiles for the Si/CdS core-shell. Figure 14f shows the best fit and includes a small concentration of Si in the shell. This

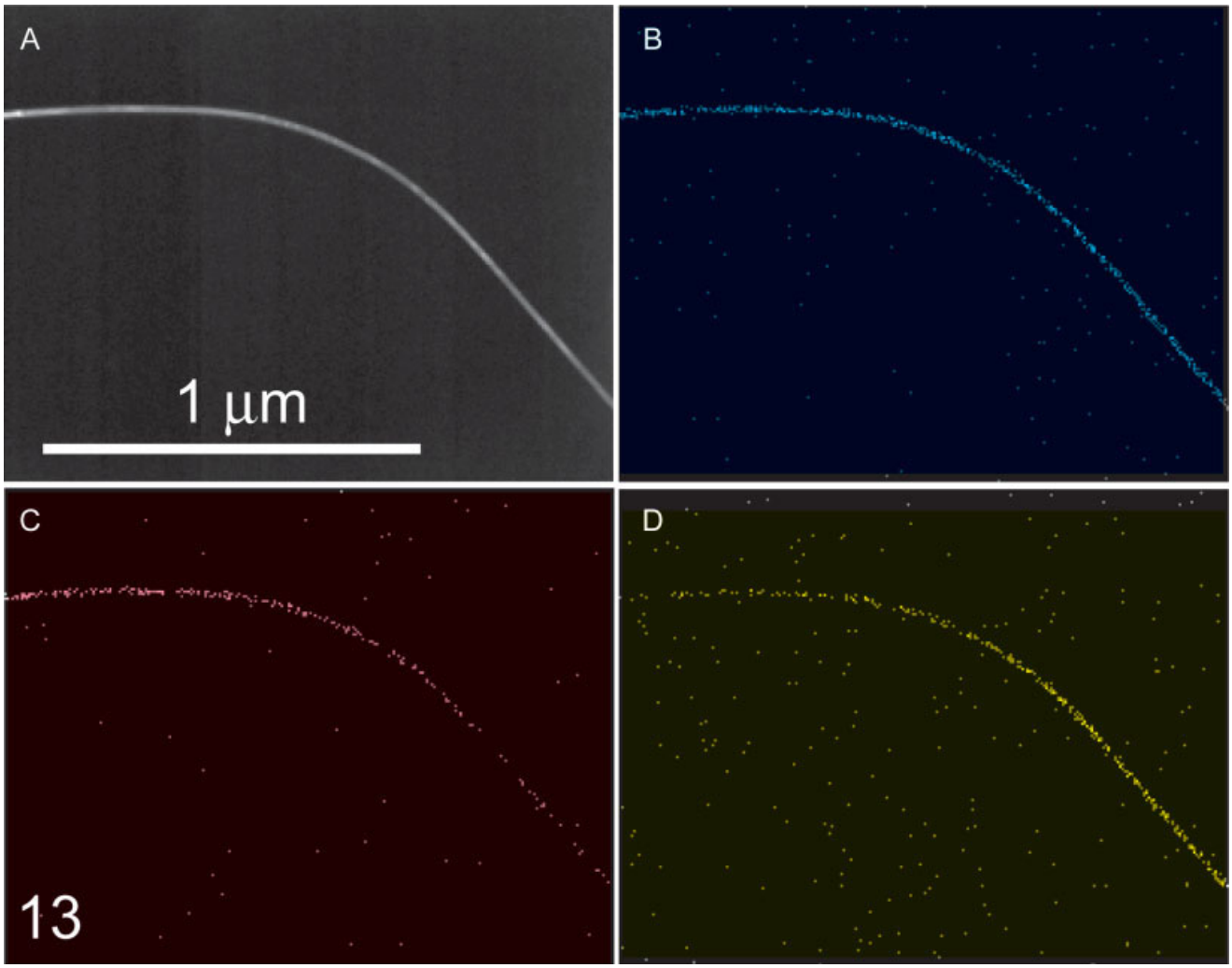

Fig. 13. Images of a ZnS/ZnSe nanowire obtained using scanning transmission electron microscopy (STEM). **a:** Darkfield STEM image of a ZnS/ZnSe nanowire. **b:** Elemental mapping of the zinc X-ray intensity compositing along the nanowire. **c:** Elemental mapping of the selenium compositing along the wire. **d:** Elemental mapping of the sulfur compositing along the nanowire.

experiment demonstrates that Gaussian fitting procedures are readily suitable for analysis of nanowire systems in which the core and shell are made from distinct materials.

DISCUSSION

HRTEM Imaging

The HRTEM imaging and analysis of discrete single-element nanowires and more complex nanowire heterostructures presents the researcher with distinct challenges. As always, the interpretation of atomic structure images obtained by HRTEM requires consideration of the physics involved in imaging and, in the case of imaging nanowires, the effects of a "finite" crystal size (and hence not a completely periodic structure). Also, because of the large reciprocal space function (due to the diameter of the wires), HRTEM imaging requires the careful consideration of possible artifacts and diffraction effects before conclusions as to the structure of the wire can be made. We believe that for complete understanding a model of the nanowire or nanowire heterostructure should be constructed based on the diffraction, HRTEM structure images, and image simulations, such as for our nanowires (Wu et al., 2004a,b).

Determination of the nanowire growth direction is one element required to construct a model of the nanowire structure and to help provide insight into the dynamics of nanowire growth during the synthesis process. Determination of the crystal growth direction follows from Williams and Carter (1996); for determination of the growth direction of nanowires we recorded and indexed the nanowire selected area diffraction pattern from a planar wire tilted to a zone-axis and compared the diffraction pattern orientation relative to the nanowire image. The lattice spacing in the HRTEM structure image can also be

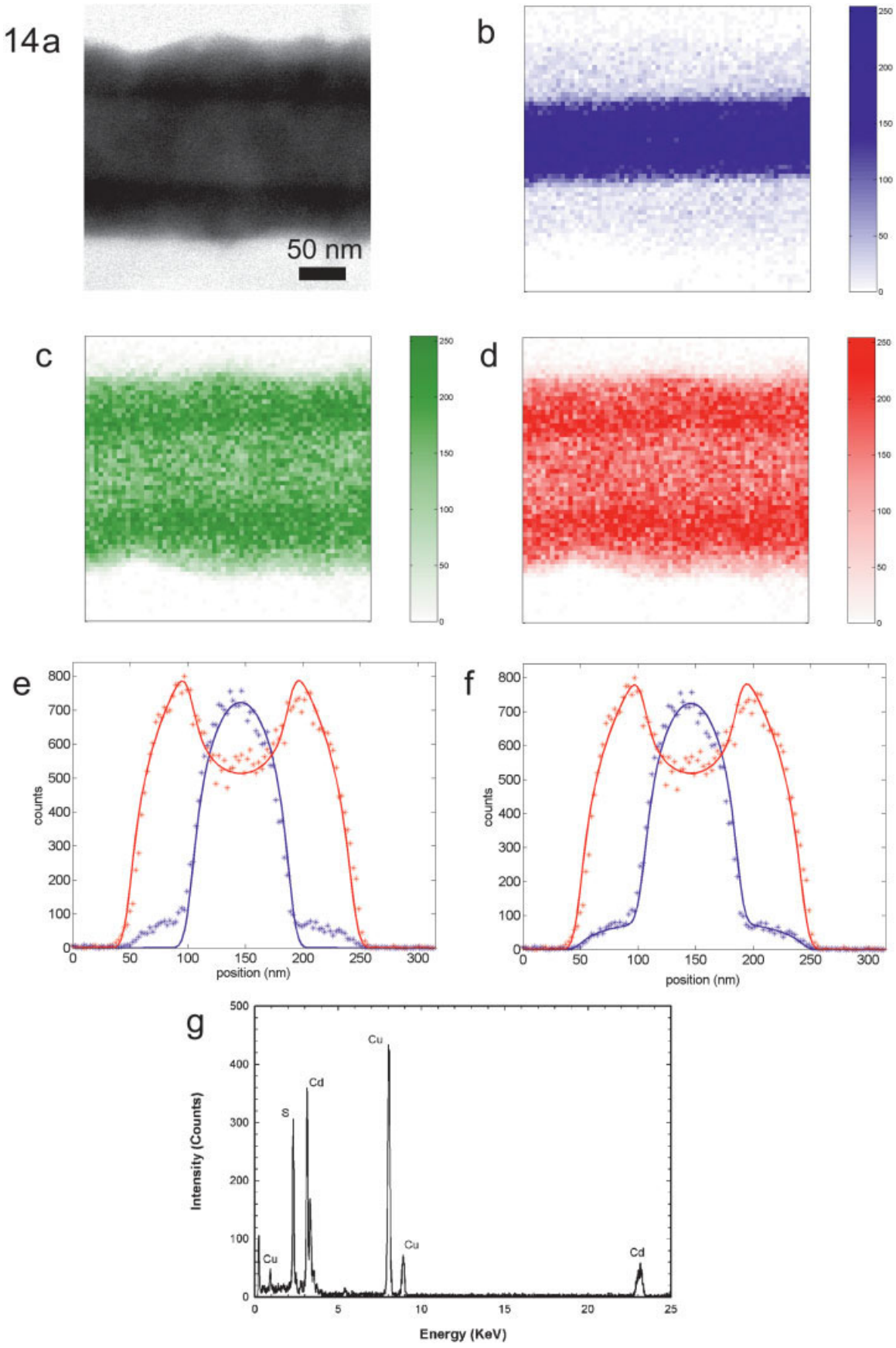
14a
50 nm
b
c
d
e
counts
position (nm)
f
counts
position (nm)
g
Intensity (Counts)
Energy (KeV)
Cu
S
Cd
Cu
Cu
Cd

Fig. 14.

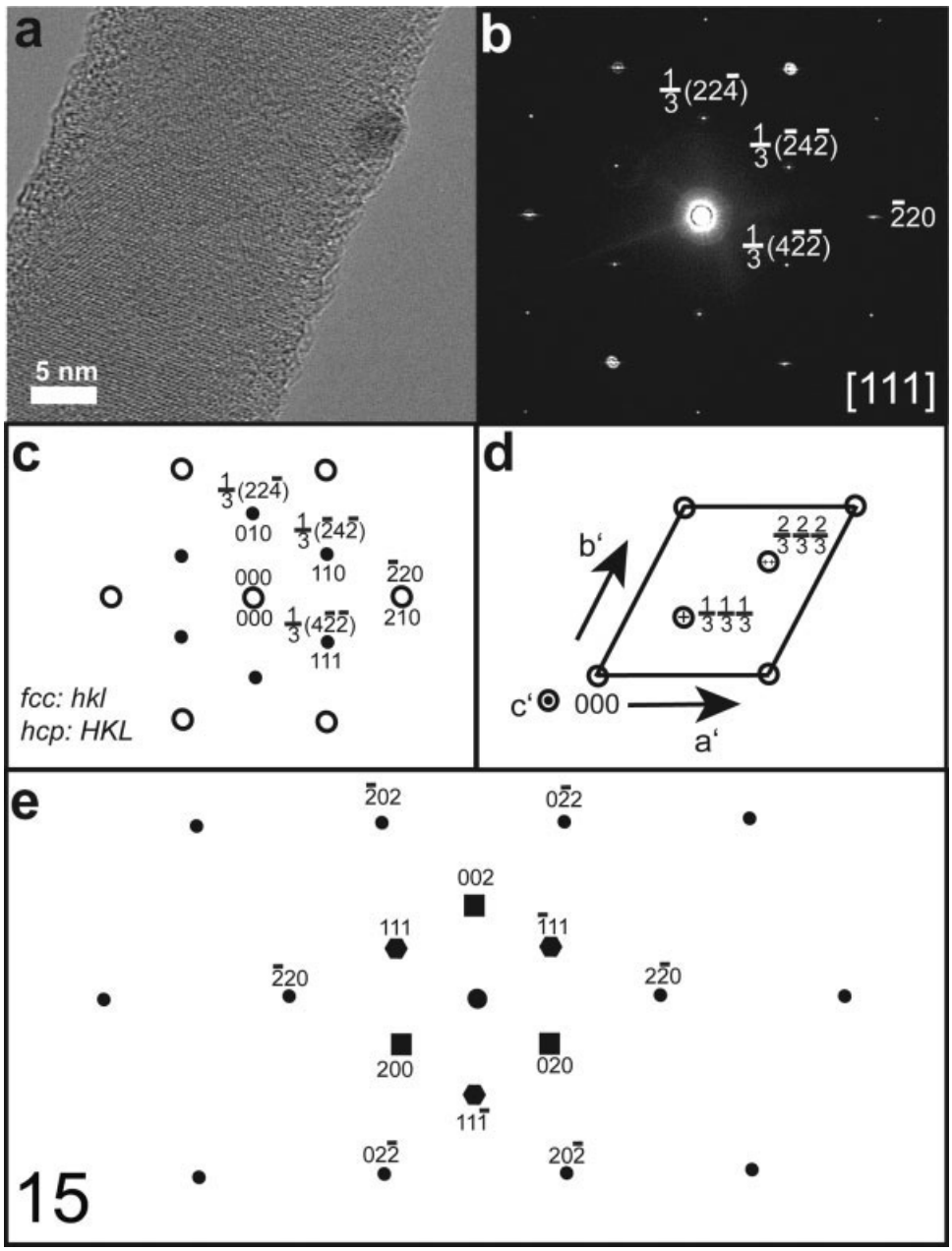

Fig. 15. Anomalous diffraction in silicon nanowires along the [111] zone axis. **a:** HRTEM image of a silicon nanowire with [111] zone axis. **b:** The corresponding diffraction pattern with indexed reflections. **c:** Hexagonal unit cell for an fcc structure. The a' and b' are in the plane of the (111) (cubic notation) of the fcc crystal and c' is normal to the a'b' plane. $c' = \leftrightarrow \sqrt{6}b' = \sqrt{6}a'$. **d:** Reciprocal lattice points along the [001] axis of the hcp unit cell and [111] of the fcc unit cell. **e:** Projection of [111] zone fcc crystal reciprocal lattices onto the zero order zone plane. Circles: zero-order; triangles: first-order; squares: second-order Laue zone.

used to assist in determining growth direction. (It should be noted that for some TEMs it is first necessary to perform a calibration using a crystal such as MgO to determine image rotation relative to the diffraction pattern.) The growth direction of the nanowire will lie orthogonal to the observed crystal zone-axis and be in the direction of the Bragg reflection that corresponds to the nanowire length. For example, as in Wu et al. (2004b), if a silicon nanowire is imaged along the [111] zone axis and the nanowire direction corresponds to the (110) direction, then we know that the nanowire growth occurs along the

Fig. 14. Scanning transmission electron microscope (STEM) images including EDS spectrum imaging from a CdS/Si core-shell structure. **a:** Brightfield image of the nanowire. **b:** Extracted Si-K X-ray intensity image. **c:** extracted Cd-L X-ray intensity. **d:** Extracted S-K X-ray intensity. **e:** Cd-L (red) and Si-K (blue) line profiles; markers are measured values and solid lines are calculated profiles for Si/CdS core-shell structure in which the calculations do not assume Si in the shell. **f:** Same as **e**; however, the best fit includes small concentration of Si in the shell. **g:** EDS spectrum of overall CdS nanowire; note the low total counts. The characteristic Cu X-ray peaks are due to scattering from the TEM support grid.

{110} family of lattice planes. As an additional check the same nanowire can also be tilted axially to another zone-axis orientation and the growth directed again determined.

We also discovered, by employing the modeling methods as described above and confirmed by preparing and imaging nanowire cross-sections, that most nanowires have surfaces that are faceted (Wu et al., 2004a). This faceting of the wire surface most likely explains why the typical HRTEM structure images of thin <20 nm nanowires show a central core area that appears in images as distinctly crystalline, whereas the edges can appear amorphous or at least with differing phase contrast. Further study is needed to confirm this hypothesis and develop HRTEM image simulation methods that take nanowire faceting into account for thin nanowires.

Anomalous Diffraction From Nanowires

For certain silicon nanowire orientations, the diffraction patterns obtained differ from a corresponding bulk silicon pattern with the same zone-axis orientation. As mentioned above, the diffraction pattern from a thin silicon nanowire (Fig. 15a) taken along the [111] zone axis showed additional reflections a short reciprocal distance from the transmitted beam (Fig. 15b). Such reflections were first observed for silicon nanowires by Gudiksen (2002) and have been observed in other nanoscale materials such as gallium oxide nanoribbons by Dai et al. (2002). Other studies of cubic materials imaged with TEM along the [111] zone axis also show low intensity reflections that can be indexed to the $\frac{1}{3}\{\bar{4}22\}$ family of lattice planes such as Xiao and Daykin (1994). The $\frac{1}{3}\{\bar{4}22\}$ family of planes are forbidden in a corresponding bulk crystal, for which the lattice can be considered infinite. Selected area electron diffraction patterns of silicon nanowire samples of up to ~60 nm in diameter shows the same pattern, with bright {220} spots and six smaller anomalous spots with weaker intensity inside the {220}. The spots that correspond with the type $\frac{1}{3}\{\bar{4}22\}$ and have also been seen in [111] diffraction from fcc films such as gold or silicon (Morris et al., 1968; Gibson et al., 1989).

We propose that there are two compounding reasons why these classically forbidden reflections appear so prominently in our recorded nanowire diffraction patterns. The first reason is that because the reciprocal space function of the nanowire along the beam direction is large, due to the thinness of the wire, the interception of Ewald sphere by the diffracted beams increases the intensity transfer of any individual diffracted beam. The second reason is due to the nature of the nanowire object itself: physically, edge effects become important and noticeable as compared to diffraction from a bulk or effectively infinite thin film crystal lattice.

Our proposed explanation of this effect is as follows: silicon has a diamond structure, which consists of two sets of fcc lattices of Si offset by $\frac{1}{4}$ lattice spacing along the [111] direction. An fcc unit cell has four lattice points and an easy analysis of the diffraction structure factor F_{hkl} gives only reflections from all even or all odd (hkl) lattice planes that have nonzero intensity. In silicon, each basis contains two identical silicon atoms at (0,0,0) and $(\frac{1}{4},\frac{1}{4},\frac{1}{4})$, therefore allowing only reflections if h,k,l are all odd or even and h+k+l is a multiple of 4. The silicon nanowire diffraction pattern shown in Figure 15b shows a set of six diffraction spots which appear inside the {220}, while the {220} is the smallest set of spots kinematically allowed in [111] zone axis of a bulk fcc crystal, as discussed above.

One proposed origin of these anomalous diffraction spots can be explained by unequal numbers of the A, B, and C hexagonal planes perpendicular to [111] direction in an fcc crystal. It can be better understood if we choose a hexagonal hcp unit cell instead of a cubic one for an fcc crystal as in Figure 15d (Cherns, 1974). In such an hcp unit cell, each cell contains three scattering centers, at (0,0,0), $(\frac{1}{3},\frac{1}{3},\frac{1}{3})$, and $(\frac{2}{3},\frac{2}{3},\frac{2}{3})$, which corresponds to the three successive layers ABC. The reciprocal lattice from a [001] or c' axis in the hcp notation can be viewed in Figure 15c. Figure 15c suggests that the $\frac{1}{3}\{\bar{4}22\}$ reflection seen in silicon nanowires could originate from the (100) and (010) reflection in the hexagonal plane.

The structure factor for the hcp unit cell depicted in Figure 15d can be easily calculated to be:

$$F_{hkl} = f(\theta)\,(1 + \exp[2\pi i\,(h + k + l)/3] + \exp[4\pi i\,(h + k + l)/3])$$

which describes that only h+k+l=3n reflections will have nonzero intensity. In Figure 15b it appears that the (100) and (010) are again forbidden. Importantly for a nanowire with small diameter and near spherical cross-sectional shape, the number of ABC layers is finite and it would be expected that there will be incomplete unit cells with only A or AB planes. If we consider one of the forbidden $\frac{1}{3}\{\bar{4}22\}$ type reflection and sum up all the unit cell column along the c' direction (normal to the plane as shown in Fig. 15d), then the column structure factor would be:

$$\mathrm{F} = f(\theta)\sum_{1}^{3n} \exp[2\pi i n]$$

where n is the number of unit cells along c' and does not have to be an integer. The sum from 1 to 3n is over all ABC planes in the column. Therefore, it is obvious that if n is an integer, then all unit cells are complete and F will be zero but it is nonzero for $n = m \pm \frac{1}{3}$, and it explains the observation of forbidden diffraction spots in silicon nanowires. In the language of the multislicing method, if we choose a slice thickness to be 1/3c' instead of c', then each successive three slices has a translational offset of $(\frac{1}{3},\frac{1}{3},\frac{1}{3})$ with respect to each other. By using a Fourier transform, this offset leads to 120° phase change in phase grating through each of the three slices. Thus, a total of 3m slices will generate only an identity transformation and therefore no anomalous spots, while $3m \pm 1$ slices will lead to finite intensity at the anomalous spots similar to diffraction on a single closed-packed atom layer.

An alternative approach to understand the anomalous diffraction spots in silicon nanowires is to view the forbidden in-zone reflection spots as higher-order Laue zone reflections (Cherns, 1974; Lynch, 1971) where the

s_z (interaction distance) at the forbidden spots is so large that it is equal to 1/c'. Figure 15e illustrates the relative position of the projection of the first and second Laue zone reflections onto the zero-order zone plane. It shows that the observed finite intensity in the forbidden zero-order zone spots can be assigned to the higher-order Laue zone diffraction of $\{111\}_1$ and $\{002\}_2$.

The existence of higher-order Laue diffractions as anomalous diffraction spots has been illustrated by an experiment on gallium oxide nanobelt structures, which are also a family of high aspect-ratio quasi-1D nanostructures, having a thickness of only 10–60 nm (Dai et al., 2002). Typical diffraction patterns taken from a single Ga_2O_3 nanobelt along [101] shows the reflections with strong intensity are determined to be zero-order Laue zone reflections. However, a set of smaller, weaker reflection spots can also be observed which do not belong to any of the allowed zero-order spots, but rather, can be explained by first-order Laue reflection. The appearance of this high-order Laue zone reflection is because the nanobelt sample is so thin that the elongated "reciprocal rod" is long enough to be intersected by the Ewald sphere. A further reason contributing to this observation is that the lattice spacing $d_{(100)}$ is very large in gallium oxide, so the (100) spot in reciprocal space is very close to the origin, since [100]* is almost parallel to the zone axis [101], with only 13° difference; the first-order Laue zone in reciprocal space containing (100) is very close in spacing with zero-order Laue zone, both of these effects contribute to the ease of observing the higher order Laue reflection in the diffraction pattern.

Nanowire Microanalysis

As previously mentioned, microanalysis of synthesized nanowires and nanowire structures is important for several reasons: to understand the nature of the wires themselves, to provide a feedback mechanism to further enhance the development of nanowire synthesis, and to examine modes of synthesis failure. The most frequently used form of microanalysis is energy dispersive X-ray spectroscopy (EDS); because of the ultrasmall nature of the nanowires the analysis is commonly carried out in a TEM or STEM. Basic qualitative compositional analysis using a TEM is achieved by focusing a probe on the sample in imaging mode and examining the EDS spectrum. The advantage of this method of operation is that imaging and analysis can be performed at the same time or at least during the same microscope session. Nanowire EDS analysis is best conducted with either a dedicated STEM or a TEM/STEM operating in STEM mode. A detailed understanding of the synthesized nanowire or nanowire device requires: knowledge of what the wire is made of, analysis of whether the synthesis components that formed the wire ended up in the expected locations and in the correct quantities, and finally a determination of the sufficiency of the quality of the finished wire for the intended device purpose. For example, in the case of a nanowire core-shell structure it is important to know that the shell structure is uniform and complete. Microanalysis is also essential to determine levels of reaction by-products and the identification of possible contamination in the nanowire or device.

One of the required features in a semiconductor heterostructure is abrupt compositional or structural transition between different semiconductor regions. In the mature field of planar semiconductors, electron microscopy techniques have been developed that allow investigation of strains, chemical, and structural composition on a nanoscale. For planar semiconductor structures, where the thickness of TEM thin foils does not vary significantly over the region of interest, high-resolution TEM (Rosenauer, 2003) and electron energy-loss spectroscopy (EELS) (Leifer et al., 2000) techniques are suitable for determination of composition and strains or identification of point defects (Gradecak et al., 2002). However, these methods are not readily applicable for study of nanostructures in which the chemical composition changes simultaneously with the sample thickness. Similar problems are faced when chemically sensitive TEM techniques like dark-field or weak-beam imaging are used.

In a STEM, a finely focused electron beam (typically with a diameter of less than 5 nm) scans across the nanowire sample. Transmitted, secondary, back-scattered, and diffracted electrons as well as the characteristic X-ray spectrum can be observed. By evaluation of the EDS spectrum, the information of the distribution of different composition in complex nanowire structure can be retrieved by either extracting an EDS line profile first by doing a line scan along or across the nanowires or to construct spectrum images of different elements (also known as elemental mapping) by collecting X-ray signals over a defined area.

Experimental considerations are critically important for successful nanowire analysis; in the case of EDS analysis, with a fine <3 nm electron probe it is more prudent to limit the probe current to reduce damage of the sample and collect for longer duration than to maximize probe current, as is the normal procedure. Beam damage caused by the electron probe on a typical nanowire sample can easily cut into the wire and actually break the wire, so test runs of differing probe currents and size are needed to optimize detector count rate but leave the wires intact. Generally required microscope conditions for microanalysis follow from Garratt-Reed and Bell (2003); issues to avoid include shadowing effects and to understand the EDS geometry considerations to ensure that the sample presents a planar view to the location of the EDS detector in the microscope. If performing line scans or spectrum imaging the nanowire must be aligned to present a uniform aspect ratio to the detector along all points of the scanned area, failure to understand the geometry of the analysis results in acquiring data where the effects of the sample aspect ratio change can be misinterpreted as compositional changes along the wire length or around the radius.

Collected EDS spectra are analyzed by identifying the characteristic X-ray peaks, subtracting the EDS background, and performing a peak quantification (commercial software packages are available suitable for large dataset analysis, but special care should be taken during this procedure to avoid quantification artifacts). In the first approximation for nanowires with relatively small thickness, when absorption effects are neglected, intensity of an elemental peak can be considered as proportional to the volume containing

the specific element and excited by an electron beam. The general morphology and approximate cross-section hence have to be determined with imaging methods prior to EDS analysis to allow correct modeling of the sample thickness, and therefore EDS intensity, along the line profile. In this sense, double tilt stages with large tilt angles and/or cross-section TEM samples are of great help. Quantitative line profiles can be readily modeled by assuming a Gaussian electron probe profile. From these measurements thickness of the core and shells in the core-shell nanowires can be calculated (for noncylindrical nanowires the line profile would depend on the sample orientation toward an electron beam). Reabsorption effects should be taken into account when interpreting quantitative results and estimating the concentration of more complex structures, in which one element might be present in both core and the shell.

CONCLUSIONS

Electron microscopy will continue to play an important role in the further development of nanotechnology and nanomaterials. Further enhancements of electron microscope instrumentation as well as the corresponding refinements of electron microscopy methods and techniques will lead to greater understanding of material fundamentals of nanoscale devices and synthesis methods. Imaging and analysis of nanowire-based nanotechnology follows from traditional high-resolution and analytical electron microscopy methods; however, we have shown the need for modifications to the procedures because of the nanoscale dimensions of the samples involved.

Nanowire syntheses are based on the vapor-liquid-solid (VLS) growth mechanism in which a nanocluster is used as a catalyst, and then exposed to a vapor precursor that initiates through alloying a crystal nucleation process to grow the nanowire. More complex nanowire devices are possible with modification of the synthesis methods and compositionally modified heterostructures can be formed either along the wire, termed a nanowire axial heterostructure, or radially as a core-shell heterostructure.

Techniques for HRTEM of nanowires and nanowire-based devices must correspondingly account for the finite size of the sample, and the effects on the crystal structure due to electron beam irradiation. Knowledge of the crystal structures involves a corresponding understanding of the effects that the large reciprocal space function of the wire have on the analysis. Tilting of the nanowires to a zone-axis alignment for HRTEM requires the use of high-order reflections for correct orientation. Forbidden reflections are also possible when recording diffraction patterns from the nanoscale objects due to crystal thickness and composition. HRTEM multislice image simulation routines need modification to incorporate the effects of finite sample width, as well as the possibility of "incorrect lattice spacings" being present in the HRTEM structure image.

Scanning electron microscopy techniques have been shown to be critical to the microanalysis of nanowires and nanowire-based devices, with spectral imaging necessary to quantify and successfully fabricate nanodevices or understand modes of synthesis failure. The future of nanotechnology development is fundamentally dependent on the techniques of high-resolution electron microscopy and microanalysis.

ACKNOWLEDGMENTS

The authors thank Anthony J. Garratt-Reed at the Center for Materials Science and Engineering at MIT for assistance and the use of the Vacuum Generators HB-603 STEM.

REFERENCES

Barrelet CJ, Wu Y, Bell DC, Lieber CM. 2003. Synthesis of CdS and ZnS nanowires using single-source molecular precursors. J Am Chem Soc 125:11498–11499.
Bell DC, Wu Y, Barrelet CJ, Lieber CM. 2003. Imaging nanotechnology. Microsc Microanal 9(suppl 2):284–285.
Cherns D. 1974. Direct resolution of surface atomic steps by transmission electron microscopy. Philos Mag 30:549.
Cui Y, Lieber CM. 2001. Functional nanoscale electronic devices assembled using silicon building blocks. Science 291:851–853.
Cui Y, Lauhon LJ, Gudiksen MS, Wang J, Lieber CM. 2001. Diameter-controlled synthesis of single-crystal silicon nanowires. Appl Phys Lett 78:2214–2216.
Dai ZR, Pan ZW, Wang ZL. 2002. Gallium oxide nanoribbons and nanosheets. J Phys Chem B 106:902–904.
Duan X, Huang Y, Cui Y, Wang J, Lieber CM. 2001. Indium phosphide nanowires as building blocks for nanoscale electronic and optoelectronc devices. Nature 409:66–69.
Garratt-Reed AJ, Bell DC. 2003. Energy-dispersive X-ray analysis in the electron microscope. London: BIOS Scientific (US distributor, Springer).
Gibson JM, Lanzerotti MY, Elser V. 1989. Plan-view transmission electron diffraction measurement of roughness at buried Si/SiO2 interfaces. Appl Phys Lett 55:1394–1396.
Gradecak S, Wagner V, Ilegems M, Riemann T, Christen J, Stadelmann P. 2002. Microscopic evidence of point defect incorporation in laterally overgrown GaN. Appl Phys Lett 80:2866–2868.
Gudiksen MS. 2002. Semiconductor nanowires and nanowire heterostructures: development of complex building blocks for nanotechnology. Ph.D. Thesis, Harvard University, Cambridge, MA.
Gudiksen MS, Lieber CM. 2000. Diameter-selective synthesis of semiconductor nanowires. J Am Chem Soc 122:8801–8802.
Hu J, Odom TW, Lieber CM. 1999. Chemistry and physics in one dimension: synthesis and properties of nanowires and nanotubes. Acc Chem Res 32:435–445.
Huang MH, Mao S, Feick H, Yan H, Wu Y, Kind H, Weber E, Russo R, Yang P. 2001a. Room-temperature ultraviolet nanowire nanolasers. Science 292:1897–1899.
Huang Y, Duan X, Cui Y, Lauhon LJ, Kim K, Lieber CM. 2001b. Logic gates and computation from assembled nanowire building blocks. Science 294:1313–1317.
Iijima S. 1991. Helical microtubules of graphitic carbon. Nature 354: 56–58.
Lauhon LJ, Gudiksen MS, Wang D, Lieber CM. 2002. Epitaxial core-shell and core-multishell nanowire heterostructures. Nature 420: 57–61.
Leifer K, Buffat PA, Stadelmann PA, Kapon E. 2000. Theoretical and experimental limits of the analysis of III/V semiconductors using EELS. Micron 311:411–427.
Lichte H. 1991. Optimum focus for taking electron holographs. Ultramicroscopy 38:13–22.
Lieber CM. 2003. Nanoscale science and technology: building a big future from small things. MRS Bull 28:486–491.
Lynch DF. 1971. Out of zone effects in dynamic electron diffraction intensities from gold. Acta Cryst A27:399.
Malm J-O, O'Keefe MA. 1997. Deceptive "lattice spacings" in high-resolution micrographs of metal nanoparticles. Ultramicroscopy 68: 13–23.
Morris RH, Bottoms WR, Peacock RG. 1968. Growth and defect structure of lamellar gold microcrystals. J Appl Phys 39:3016–3021.
Nihoul G, Sack-Kongehl H, Urban J. 1998. Electron microscopy structural characterization of nano-materials: image simulation and image processing. Cryst Res Technol 33:1025–1037.
Otten MT, Coene WMJ. 1993. High-resolution imaging on a field emission TEM. Ultramicroscopy 48:77.
Rosenauer A. 2003. Transmission electron microscopy of semiconductor nanostructures. Heidelberg: Springer.

Spence JCH. 1981. Experimental high resolution electron microscopy. Oxford: Oxford University Press.
Stadelmann PA. 1987. EMS—a software package for electron-diffraction analysis and HREM image simulation in materials science. Ultramicroscopy 21:131–145.
Stadelmann PA. 1995. Electron microscopy image simulation online Java version, http://cimewww.epfl.ch/people/stadelmann/jemsWebSite/jems.html
Wang J, Gudiksen MS, Duan X, Cui Y, Lieber CM. 2001. Highly polarized photoluminescence and photodetection from single indium phosphide nanowire. Science 293:1455–1457.
Williams DB, Carter CB. 1996. Transmission electron microscopy. New York: Plenum Press.
Wu Y, Yang P. 2001. Direct observation of vapor-liquid-solid nanowire growth. J Am Chem Soc 123:3165–3166.
Wu Y, Xiang J, Yang C, Lu W, Lieber CM. 2004a. Single-crystal nanowires and metal/semiconductor nanowire heterostructures. Nature 430:61–65.
Wu Y, Cui Y, Huynh L, Barrelet CJ, Bell DC, Lieber CM. 2004b. Controlled growth and structures of molecular-scale silicon nanowires. Nano Lett 4:433–436.
Xiao HZ, Daykin AC. 1994. Extra diffractions caused by staking faults in cubic crystals. Ultramicroscopy 53:325–331.
Zhong Z, Wang D, Cui Y, Bockrath MW, Lieber CM. 2003. Nanowire crossbar arrays as address decoders for integrated nanosystems. Science 302:1377–1379.